

Anderson-Localization and the Mott–Ioffe–Regel Limit in Glassy-Metallic PEDOT

*Dominik Farka, Halime Coskun, Jacek Gasiorowski, Christoph Cobet, Kurt Hingerl, Lisa Maria Uiberlacker, Sabine Hild, Theresia Greunz, David Stifter, Niyazi Serdar Sariciftci, Reghu Menon, Wolfgang Schoefberger, Cezarina Cela Mardare, Achim Walter Hassel, Clemens Schwarzingler, Markus Clark Scharber, and Philipp Stadler**

Conductive polymers represent a rare case in which free-carrier absorption is shifted to the far-infrared—an attractive advantage in light of the requirement of highly transparent conductors across the visible and near-infrared. Unfortunately, prior approaches to doping these polymers—imperative for high conductance—have consistently led to strong localization arising from fluctuating band alignment among polymer chains. Here, this study overcomes this problem of doping-induced Anderson localization for the first time in polymers by developing a new conductive polymer synthesis strategy. This study achieves polymerization and doping simultaneously, thereby using an alternative nonmetal oxidant and thereby avoiding the introduction of excess energy that normally arises from exergonic polymerization. The resulting conductive polymer is the first to provide electron coherence in a metallic polymer thin film. The conductivity reaches a remarkable 3300 S cm^{-1} at 1.8 K and the mean electron scattering length a record 330 \AA . This enhancement drives the glassy metal transition in the vicinity of the Mott–Ioffe–Regel (MIR) limit. The new metallic polymer achieves $10^{-2} \Omega^{-1}$ figure of merit, making it a contender for transparent conductive contacts previously only accessible using inorganics. The new material offers a uniquely broad transparency window spanning the UV to the mid-infrared.

There exists a tremendous interest in metallic polymers as they combine facile processing, high conductivity and transparency. However, to date no straightforward method has been found to engineer a system that unites high doping and high order.^[1–6] The apparent conflict lies in the nature of doping of a conducting polymer, which occurs through a distinct mechanism compared to inorganic semiconductors. Severe lattice distortions arise in the doping of conducting polymers as a result of the penetration of ions into the system. Consequently, the solid-state order becomes disrupted—it transforms from a former homogeneous organic van der-Waals crystal into a disordered salt. To form a substantial degree of order, growth methods have to consider the effect of ion penetration.^[7–16]

Small molecular systems have the advantage that they can be dissolved in polar solvents. Thus they can be grown in the doped form as a salt dissolved from

D. Farka, H. Coskun, Prof. N. S. Sariciftci, Dr. M. C. Scharber, Dr. P. Stadler
 Linz Institute of Organic Solarcells (LIOS), Institute of Physical Chemistry
 Johannes Kepler University Linz
 Altenberger Strasse 69, 4040 Linz, Austria
 E-mail: philipp.stadler@jku.at

Dr. J. Gasiorowski, Dr. C. Cobet, Prof. K. Hingerl, T. Greunz, Dr. D. Stifter
 Center for Surface and Nanoanalytics
 Johannes Kepler University Linz
 Altenberger Strasse 69, 4040 Linz, Austria

Dr. J. Gasiorowski
 Department of Physics
 Technical University of Chemnitz
 Reichenheiner Strasse 70, 09126 Chemnitz, Germany


L. M. Uiberlacker, Prof. S. Hild
 Institute of Polymer Science
 Johannes Kepler University Linz
 Altenberger Strasse 69, 4040 Linz, Austria

Prof. R. Menon
 Department of Physics
 Indian Institute of Science
 Bangalore 560012, India

Dr. W. Schoefberger
 Institute of Organic Chemistry
 Johannes Kepler University Linz
 Altenberger Strasse 69, 4040 Linz, Austria

Dr. C. C. Mardare, Prof. A. W. Hassel
 Christian Doppler Laboratory for Combinatorial Oxide Chemistry (COMBOX) at Institute for Chemical Technology of Inorganic Materials
 Johannes Kepler University Linz
 Altenberger Strasse 69, 4040 Linz, Austria

Dr. C. Schwarzingler
 Institute for Chemical Technology of Organic Materials
 Johannes Kepler University Linz
 Altenberger Strasse 69, 4040 Linz, Austria

 The ORCID identification number(s) for the author(s) of this article can be found under <http://dx.doi.org/10.1002/aelm.201700050>.

DOI: 10.1002/aelm.201700050

solution. Such Fabre–Bechgaard salts have created an entire field of synthetic metals and superconductors.^[17–20] In polymers, however, the macromolecular nature hampers the formation of a thermodynamic solution.^[19] Consequently, conductive thin films are generated by two-step processes (first casting, then doping).^[17–37] Such methods effectively disturb the order and thus result in an Anderson insulator rather than a metallic conductor.

Oxidative chemical vapor deposition (o-CVD) is a quasi-1-step technique, where doping and polymerization are combined.^[38] State-of-the-art processes rely on vigorous reactants such as metal chlorides (FeCl₃, SbCl₅). Although the production of high-performance polymers has been demonstrated, overoxidation leads to severe structural distortions.^[39,40] Here we develop a new process that achieves superior metallic properties but overcomes the prior reliance on lattice-disrupting metal dopants. The o-CVD is performed at ambient pressure and uses nitrogen as carrier gas, which is saturated with the monomer ethylene-(3,4-dioxythiophene) (EDOT). In the reactor zone the vapor is contacted with gaseous sulfuric acid to condense as oxidatively polymerized and p-doped polyethylene-(3,4-dioxythiophene):sulfate (PEDOT:sulfate) on the substrate. The bluish, air-stable, and semitransparent thin film precipitates as homogeneous layer on the substrate. We are in particular interested in the magnetoelectric and the optoelectronic properties and the structural composition, which we present in detail in this work. We find striking results such as a temperature-coefficient typical for glassy metals close to the Mott–Ioffe–Regel (MIR) limit.^[41–43] We observe the Hall effect and calculate the mean inelastic scattering path of charge carriers. Furthermore, we present the optical dielectric function and resolve the chemical composition. The hallmark of the PEDOT:sulfate prepared by o-CVD with sulfuric acid is the excellent electrical performance manifested by metallic fingerprints such as the positive magnetoconductivity. All these findings indicate that the new and facile synthesis route for PEDOT leads to an outstanding degree of order and purity inside the polymer with the consequence of a metallic nature beyond Anderson localization.

We choose two common chemicals EDOT and sulfuric acid in order to synthesize PEDOT:sulfate by o-CVD. The advantage of using EDOT is in particular its low oxidation potential, which can be easily overcome by sulfuric acid as oxidizing agent. By balancing the concentration and reaction, and deposition temperature we pursue an immediate, selective polymerization and avoid harsh conditions, which lead to overoxidation. With this we generate high-quality, semitransparent thin films of PEDOT:sulfate using a simple o-CVD-setup, where the quasi-1-step polymerization and doping reaction (**Figure 1**) takes place. The optimum temperature found to react EDOT readily with the vaporized sulfuric acid is 200 °C. We achieve the reaction conditions by preheating the saturated nitrogen carrier gas. The subsequent evaporation of sulfuric acid and immediate polymerization- and oxidation-reaction takes place at ambient pressure.

For comparison, we generate several reference PEDOT-systems, which originate from the classic solution-based processing routes based on the commercially available PEDOT:polystyrene sulfonate (PEDOT:PSS) dispersions. One straightforward route processes PEDOT:PSS with additives (i.e., DMSO, further denoted as PEDOT:PSS*) to reach a conductivity

value of 1000 S cm⁻¹. To obtain a similar reference system such as PEDOT:sulfate, we substitute the PSS polyanion. Therefore we treat as-deposited PEDOT:PSS with aqueous triflic acid (equimolar aqueous solution) further denoted as PEDOT:triflate.^[6] This system serves as a solution-derived reference PEDOT-system having a similar composition but different processing origin as o-CVD grown PEDOT:sulfate.^[3,44]

Similar to solution-based PEDOT:PSS, o-CVD yields homogeneous coverage on top of various substrates. Measurements of the surface morphology of films grown on glass (**Figure 1b**) show a uniform film with an average RMS-smoothness of 4.5 nm. PEDOT-fingerprint structural information is furthermore identified by ATR-FTIR, solid-state NMR and MALDI-MS, and high-resolution X-ray photoelectron spectroscopy (XPS). These studies (in detail discussed in the Supporting Information) include the reconstruction of the ratio between a monomer unit and sulfate at approximately (2.8):1, signature interaction in shifts in the ¹³C NMR, and the molar mass distribution at 10–12 EDOT units (median value) as well as characteristic interband absorptions (polarons) and infrared-activated vibrations (IRAVs).

X-ray diffraction pattern on 150 nm thin films confirm the crystallinity of PEDOT:sulfate by the (020) reflection (fingerprint for PEDOT-stacks) appearing pronounced at 25.5 2θ (3.5 Å stacking distance) (**Figure 2**). Similar features in PEDOT:triflate and PEDOT:PSS* (without and with annealing) have not been observed.

The intense peak (020) in the diffractogram relates to the excellent electrical performance of PEDOT:sulfate (outperforming all solution-derived systems across the entire temperature range between 300 and 1.8 K) (**Figure 1c**). It exhibits a room temperature conductivity as great as 4050 S cm⁻¹ (PEDOT:triflate: 2100 S cm⁻¹, PEDOT:PSS* 1000 S cm⁻¹, and PEDOT:PSS 7 S cm⁻¹), which changes slightly across the studied temperature range. At 1.8 K in the proximity of T→0 the magnitude of the conductivity displays the crucial role of disorder: As-cast PEDOT:PSS follows an Arrhenius-type temperature-activated transport and has practically 0 conductivity (**Figure 1d**). Additive-assisted PEDOT:PSS* has a finite conductivity—but a factor 10 lower as compared to room temperature. PEDOT:triflate performs similarly having an overall better performance but similar drop by a factor of 3. We used similar thicknesses to remain in a 3D bulk regime for meaningful comparison of these different kinds of PEDOT thin films.

In addition we include the resistivity versus absolute temperature ρ_T (**Figure 1e**). Thereby, PEDOT:triflate and PEDOT:sulfate display significantly the transition from an Anderson insulator to a glassy metal. ρ_T in PEDOT:sulfate remains T-independent at low T, which is characteristic for a glassy metal and similarly observed in alloys such as Al₃₃Ti₆₇. In contrast, ρ_T in PEDOT:triflate increases severely below 10 K. Furthermore, the magnitude of in PEDOT:sulfate (247 μΩ cm⁻¹) is close to the Mooij correlation or the MIR limit, which define the border between glassy and crystalline metals. Besides overcoming Anderson localization in PEDOT:sulfate, we create a conductive polymer critically close to a crystalline metal. The origin of Mooij correlation is still a mystery today, and so is the fact that the temperature coefficient of the resistivity can be negative in the apparently metallic regime approaching the Anderson transition (denoted here as glassy metal).^[41] The material synthesized here is of a very

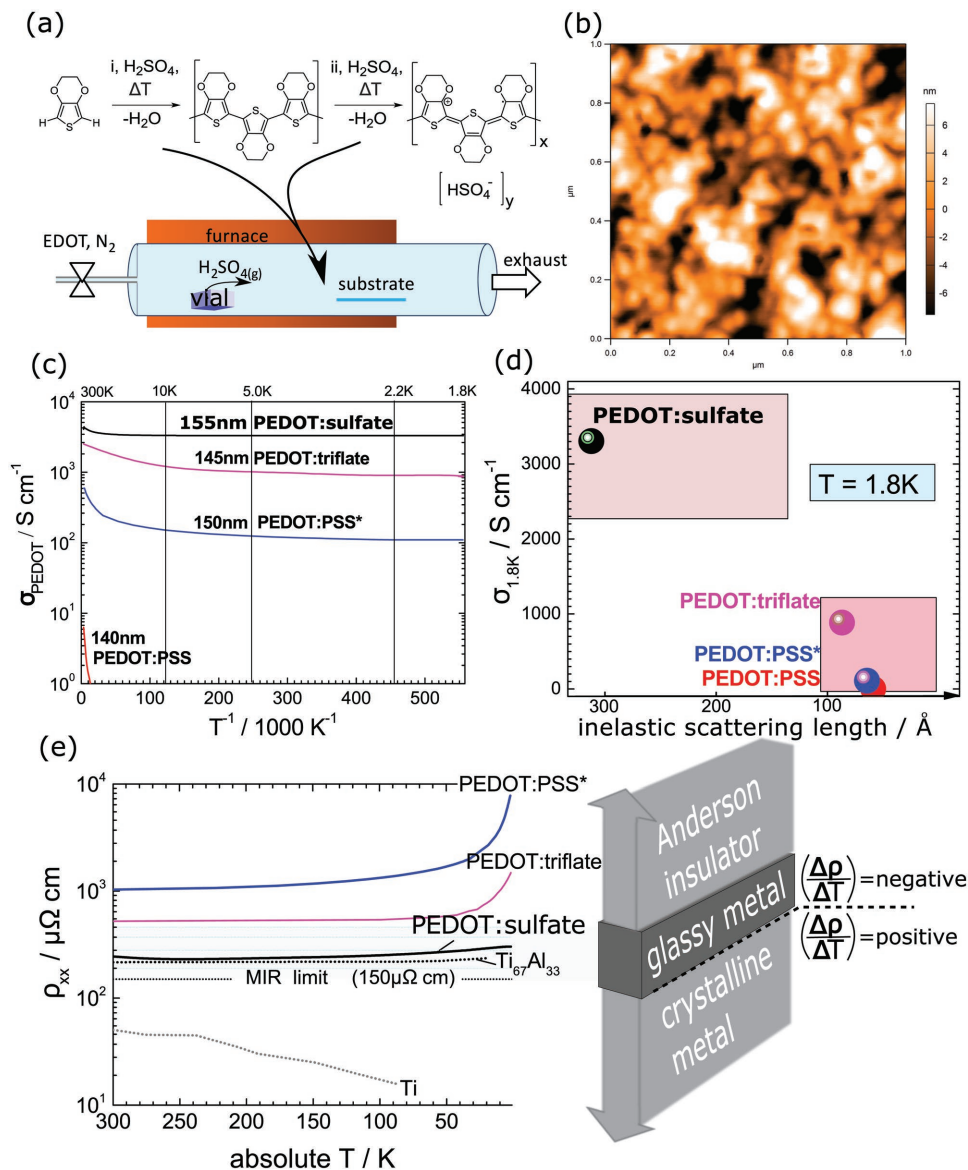


Figure 1. a) The o-CVD technique is depicted including the proposed reaction scheme of the synthesis. b) A typical surface topography of o-CVD grown PEDOT:sulfate thin film showing an RMS roughness of 4.5 nm. c) ρ_T -plot highlighting the flat T -profile of PEDOT:sulfate in particular at low temperatures. Quantitatively, the solution-based reference systems (PEDOT:PSS, PEDOT:PSS*, and PEDOT:triflate) exhibit lower performances. d) Schematic displaying the role of disorder on $\sigma_{T \rightarrow 0}$. e) MIR describes a critical resistivity (150 $\mu\Omega \text{ cm}$), at which the sign of the T -coefficient of resistivity $\frac{d\rho}{dT}$ in a metal changes (glassy to crystalline). PEDOT:sulfate is situated close to the Mott-Ioffe-Regel (MIR) limit behaving similar to glassy metal alloys such as Al₃₃Ti₆₇.

different nature from those studied by Mooij and Tsuei, yet it seems to present the same universal physics driven by the Anderson phenomenon.^[43] As such the enhancements clearly point to local order established by sulfuric-acid based o-CVD. We reach a magnitude as great as 3304 S cm⁻¹ at 1.8 K, which is a retention of 81% as compared to 300 K and a 30-fold increase in conductivity over widely used PEDOT:PSS*. In Anderson localization the conductivity changes are evaluated using the logarithmic temperature coefficient $W = -\frac{d \ln \rho}{d \ln T}$ (Figure 3). The analysis provides the discrimination of the transport mechanisms, in particular distinguishing between the critical regime of the

metal-insulator transition (W_T is constant) and the glassy metallic regime beyond Anderson localization and before MIR-limit ($W_T \ll 1$ and positive sign; W_T decreases with decreasing T). Beyond the MIR-limit W_T has a negative sign as for a crystalline metal.^[45–48] The glassy metallic regime indicated by the slope of W_T (Figure 3a) is found for PEDOT:sulfate and, less-pronounced, for solution-derived PEDOT:triflate. Comparable electrical performances in conductive polymers have previously been observed in stretch-oriented, doped polyacetylene and poly-p-phenylenevinylene.^[5,8,10–12,15,16,45–49] In addition we check the impact of a strong magnetic field ($B = 9 \text{ T}$). This allows us to switch between metallic and critical regime (magnetolocalization). In both cases,

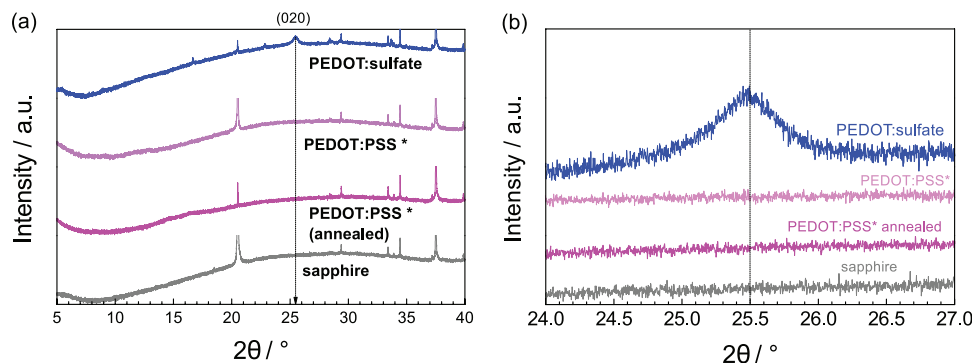


Figure 2. a) XRD on single crystalline sapphire shows the diffractograms of PEDOT:sulfate and of reference PEDOT:PSS (as-cast and annealed to 100 °C). We confirm the fingerprint peak at 25.6 2θ as observed from thin films (150 nm) on glass. The reference solution-cast PEDOT thin films are amorphous. b) (020) feature zoom of diffractogram showing details in relation to substrate (sapphire) and PEDOT:PSS* and annealed PEDOT:PSS* shows the feature at 25.5 2θ (corresponds to a stacking distance of 3.5 Å).

the magnetoeffect is consistently pronounced, as the emergence of B disrupts the metallic state seen in the constant and increased W_T -profile at 9 T. Magnetoconductivity (MC) sensitizes in particular the electron scattering mechanisms. Their mean free path reflects directly the degree of local order established in PEDOT. We apply a classic four-probe specimen (Figure 3c) to characterize the ambiguous impact of the magnetic field.^[1,5,8,10–12,15,16,49] While high fields consistently reduce the conductivity by magnetolocalization, lower magnetic fields improve the

conductivity. Such interplay is a hallmark of metallic polymers exhibiting a constructive and a destructive MC-part (Figure 3d).

The destructive-negative MC is described according to

$$\Delta\sigma_T \propto \sqrt{B} \quad (B \geq 4 \text{ T}) \quad (1)$$

Its power/magnitude is reflected in the slope of $\Delta\sigma_T$ versus $B^{0.5}$ (Figure S9, Supporting Information) and correlates with temperature T and the proximity to the metallic state (brief

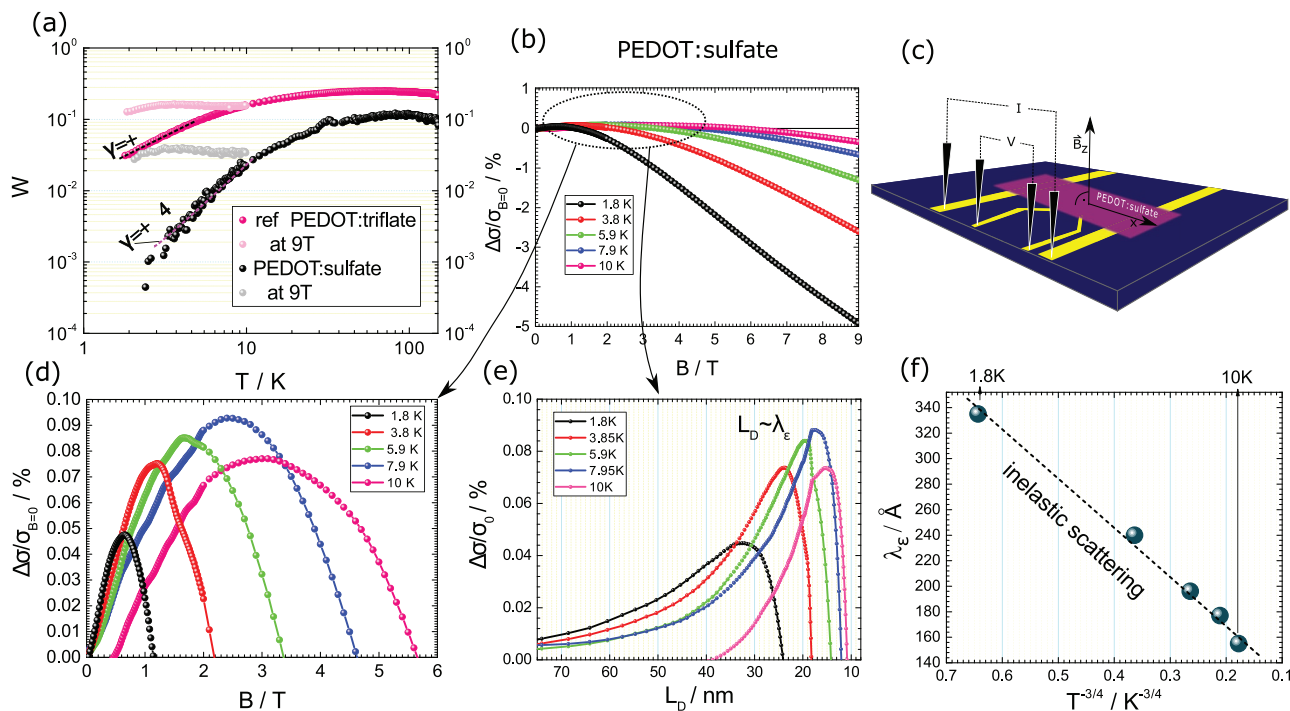


Figure 3. a) W_T -values $-\frac{d \ln \sigma}{d \ln T}$ reflect the T -dependency according to Anderson-localization (weak localization). Beyond the metal-insulator transition, W_T has a positive slope (≈ 2.4) and quantitatively approximates 0. At $B = 9 \text{ T}$ and low- T the W_T -values split due to magnetolocalization. PEDOT:sulfate has superior metallic fingerprints (quantity of W_T) as compared to the reference system (solution-based PEDOT:triflate). In (b), the magnetoconductivity (MC) of PEDOT:sulfate at five temperatures is depicted. The interference between positive (low-field) and negative (high-field) MC is shown. c) Schematic of the four-probe specimen used to characterize MCs. In (d), a zoom into the constructive MC owing to the resonance between electrons and B . e) The corresponding plot of the Landau orbit size L_D (magnetic penetration depth) and MC is used for determining the mean free path of electrons ($L_D \sim \lambda_e$) at maximum resonance. f) The linear dependence of λ_e versus $T^{-3/4}$ is characteristic for weak-localization (inelastic scattering dominates the electrical transport).

description in Supporting Information). At 10 K in the more critical regime the destructive effect is subsequently weaker (<0.5% at 9 T), while at 1.8 K (metallic regime) the conductivity decreases by 5% at 9 T.

The constructive-positive MC appears at lower magnetic fields ($B < 4$ T) and allows us to evaluate the mean free path (Figure 3e). It displays directly the electron-relaxation becoming resonant with the magnetic field B .^[48,50–53] The magnetic stimulus thereby drives a rise of the conductivity (Figure 3d). The magnetic field can be reformulated as magnetic penetration depth (the Landau orbit size L_D , Equation (2)) to read out the mean free path of scattered electrons λ_e at the peak maximum at resonance condition (Figure 3e). This is possible due to the extended scattering length found in anisotropic matter with inelastic processes dominating the transport. We denote that spin-orbit coupling effects play an insignificant role in the present system

$$L_D \approx \lambda_e \quad L_D = \sqrt{\frac{\hbar}{e \cdot B}} \quad (2)$$

In PEDOT:sulfate such resonance is seen between 1 and 6 T translating to 80 and 400 Å, respectively. Within the temperature window of 10 to 1.8 K the electrical transport is consequently coherent (Figure 3f) indicated by the fit of λ_e versus $T^{-3/4}$ characteristic for electrical transport dominated by inelastic relaxation.^[1,50]

In addition, we characterize the Hall effect using the van-der-Pauw geometry (Figure 4b). We observe the Hall potential U_{Hall} linearly arising within the coherent regime below 10 K as function of B (except for the part with B exceeding 8 T in the low temperature regime at 1.8 and 2.85 K, where destructive-negative MC disrupts the metallic phase) (Figure 4a). For evaluating the mobility from U_{Hall} (and from conductivity) we include a statistical-mechanical approach of degenerate metals. This is necessary in PEDOT:sulfate (and generally noncrystalline solids), since disorder effects can disrupt the wave functions of holes so that regular drift equations are not valid. Proper Hall models have to include the random energy distribution emerging from topological disorder.^[47,54,55] Based on drift evaluations

$$\sigma = en\mu_{\text{Drift}} \quad R_H = (en)^{-1} \quad U_{\text{Hall}} = R_H \frac{I_{xx} B}{d} \quad (3)$$

with e the electrical charge, n the carrier concentration, μ_{Drift} the drift mobility, R_H the Hall constant, I_{xx} (current), and d (layer thickness), we refer to Friedman, who proposes a random phase model (RPM), in particular for calculating the Hall conductivity in highly doped semiconductors such as PEDOT:sulfate.^[56] RPM is applicable, when λ_e exceeds molecular dimensions as demonstrated for the low- T regime. There we observe U_{Hall} arising at significant magnitude (i.e., 0.1–1 mV at $B = 5$ T) scaling (linearly) with the mean inelastic scattering lengths λ_e (or temperature) (Figure 4d). Further rising of T (e.g., above 10 K)

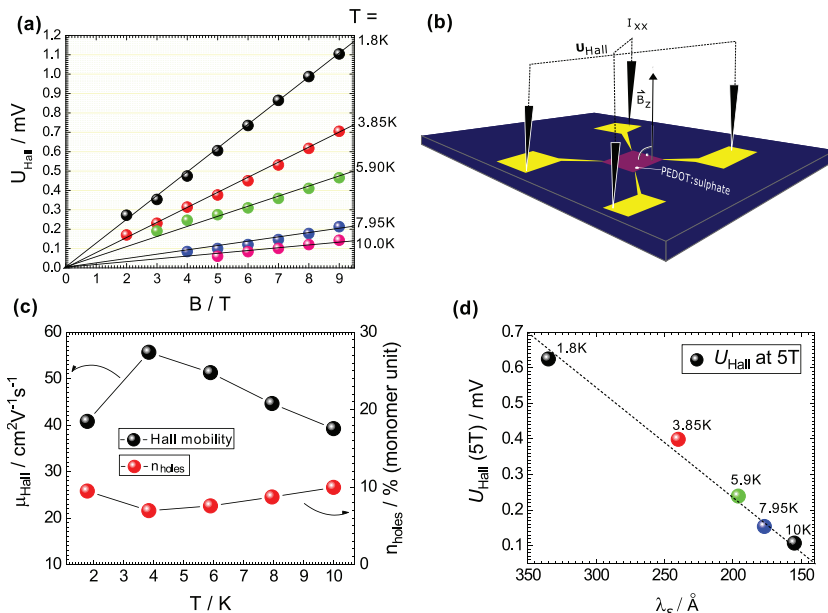


Figure 4. a) The Hall effect here shown as Hall voltage U_{Hall} arising linearly with B in PEDOT:sulfate at low- T in the metallic regime. b) Schematic of a van-der-Pauw specimen used to extract the Hall potential in eight possible geometries. c) In combination with the conductivity (i.e., 3305 S cm^{-1} at 1.8 K) the charge carrier mobility (and doping degree per monomer unit) of holes are calculated for the metallic regime below 10 K using Friedman's random phase model.^[56] d) The magnitude of the Hall potential U_{Hall} (here for B at 5 T) scales linearly with the magnitude of hole coherence (here quantified as λ_e). Lower mean free path leads to less pronounced metallic behavior (and lower Hall potential).

reduces U_{Hall} below $10 \mu\text{V}$ (the noise limit of the cryo-magneto-electric setup). We explain such behavior by localization effects becoming dominant at higher T when conductivity is governed by hopping meaning that $k_B T$ becomes greater than the band width W_B (i.e., for thermal activation). With decreasing T below 10 K hopping is effectively suppressed and conduction occurs in the band at E_F . To visualize these different transport regimes we use a semilogarithmic $\ln \sigma$ versus T^{-1} plot that reveals a T -independent (metallic) part below 10 K and the T -linear (hopping) part above 10 K (Figure S8, Supporting Information). The latter allows us to estimate the band width W_B (i.e., the activation energy) of charge carriers in PEDOT:sulfate

$$\ln \frac{\sigma_T}{\sigma_{300\text{K}}} = -\frac{W_B}{k_B T} \quad W_B \approx (E_C - E_F) = 1 \text{ meV} \quad (4)$$

These insights are particularly useful in RPM in order to evaluate Hall potentials correctly. Accordingly, drift and Hall mobilities relate by the fraction of $k_B T$ over W_B as followed

$$\mu_{\text{Hall}} = \frac{4k_B T}{W_B} \mu_{\text{Drift}} = \frac{4T}{11.3} \mu_{\text{Drift}} \quad (5)$$

We apply Equation (5) in combination with Equation (3) and now obtain constant carrier concentrations n , Hall mobilities μ_{Hall} (and conductivities) in the coherent (metallic) regime ($40 \text{ cm}^2 \text{ V}^{-1} \text{ s}^{-1}$ for μ_{Hall} and 10% free carriers per monomer PEDOT:sulfate) (Figure 4c). Note, we use the stoichiometric factor of 2.8 from XPS analysis (Figure S3, Supporting

Table 1. Electrical parameters of PEDOT:sulfate at low- T .

σ [S cm ⁻¹]	σ_r ref. σ_{300K}^a	$(eR_H)^{-1}$ [cm ⁻³]	n_{free}^b [%PEDOT:sulfate]	μ_{Hall} [cm ² V ⁻¹ s ⁻¹]	$D_{\mu V}^{c)}$ [cm ² s ⁻¹]	λ_e [Å]
1.8 K						
3305	0.81	$5.1 \cdot 10^{20}$	9.5	40.8	0.0063	335
10 K						
3336	0.82	$5.3 \cdot 10^{20}$	10	39.2	0.0338	155

^{a)} σ_{300K} is 4050 S cm⁻¹; ^{b)} n_{free} is (hole) carrier per PEDOT:sulfate monomer unit in %; ^{c)} $D_{\mu V}$ is the diffusion constant (Einstein diffusion).

Information). A detailed discussion of RPM and its application to PEDOT:sulfate is presented in the Supporting Information. In summary, we find that Hall effect in combination with MC yields congruent results pointing at the metallic transport mechanisms in the low- T regime in PEDOT:sulfate. For overview we sum up all the relevant parameters in **Table 1**.

Finally, we explore the optical properties of PEDOT:sulfate thin films to examine the transparency of PEDOT:sulfate (**Figure 5**). Our main interest is focused on the optical constants of PEDOT:sulfate between mid-IR (0.055 eV) and UV-part (6.5 eV). Therefore we use angle-resolved spectroscopic ellipsometry to generate the dielectric function $\epsilon_1(\omega)$ and $\epsilon_2(\omega)$ (**Figure 5a**). Typically for conductive polymers is the deviation

from the Drude model seen in the fingerprint mid-IR region dominated by IRAVs and electronic ingap polaron transitions. The main band-gap transition of PEDOT appears at 2.4 eV. We denote that the model used is Kramers–Kronig relation consistent. Differently to oxide-based transparent conductors the absence of a discrete plasma frequency in the investigated spectral region—we report on a consistently positive $\epsilon_1(\omega)$ upon the IRAVs—results in transparency throughout the entire spectrum. Consequently, the transmission of 30 nm PEDOT:sulfate thin film is reasonably transparent from UV to mid-infrared. Though PEDOT:sulfate has residual absorption especially in its intrinsic band gap region (**Figure 5b**), this effect is compensated with its transparency in the low-energy IR. We visualize the electro-optical performance in the complementary figure of merit according to Haacke (**Figure 5c**).^[57]

The quantity $\Phi = \sigma d \cdot TR^{10}$ from PEDOT:sulfate (TR is transmission) compared to convenient PEDOT:PSS* and to indium tin oxide (ITO), **Table 2** highlights the unique properties of transparency and conductivity over a large spectral regime. In summary, our complementary magnetoelectric and optoelectronic study on PEDOT:sulfate provides strong arguments to consider this material as serious alternative for a transparent

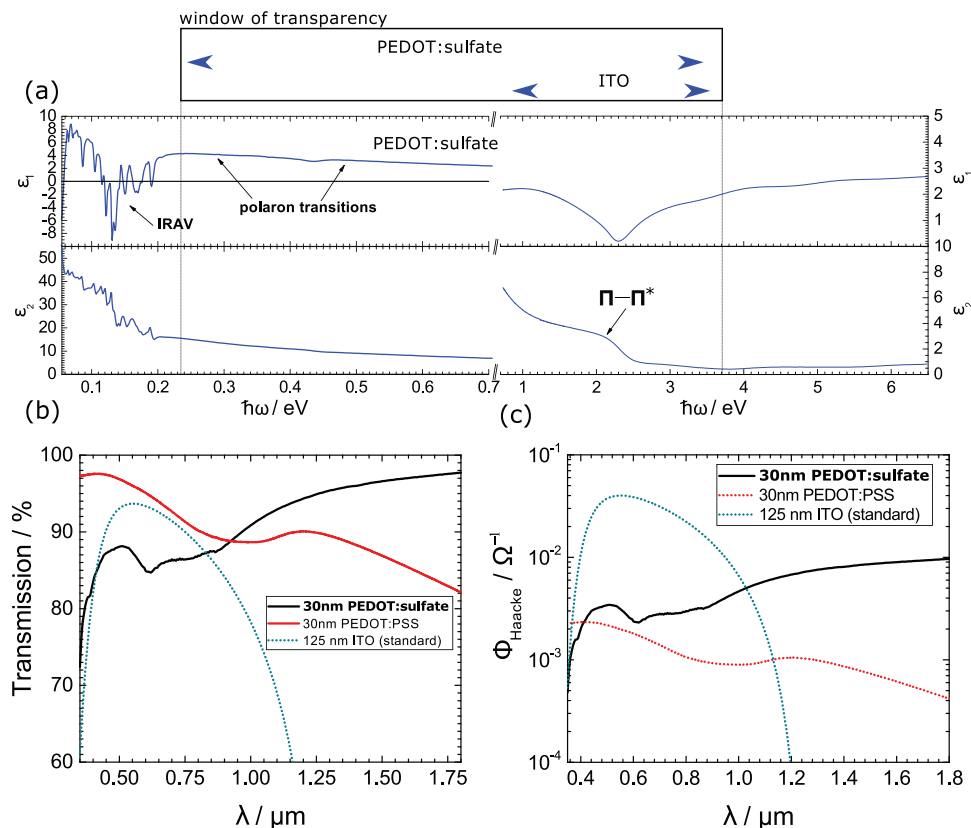


Figure 5. a) The dielectric function (experiment and model) of PEDOT:sulfate between UV- and mid-IR regime reveals the fingerprint electronic (polarons) and vibronic (IRAV) transitions. b) The latter non-Drude behavior is particularly displayed in the transmission (30 nm thin film on glass) including reference values for PEDOT:PSS. Different to ITO (plasma frequency at 0.8 eV), the window of transparency in PEDOT:sulfate is extended to the mid-infrared. c) This advantage is highlighted in the figure of merit (according to Haacke, 90% transparency) pointing at the improvements of PEDOT:sulfate as compared to PEDOT:PSS* and as compared to ITO when considering the expanded infrared-window.

Table 2. Optoelectrical parameters of PEDOT:sulfate, PEDOT:PSS*, PEDOT (FeCl₃), and indium tin oxide (ITO).

Electrode	Processing/ treatment	σ_{DC} [S cm ⁻¹]	$\Phi_{FOM,550nm}$ [Ω^{-1}]	$\Phi_{FOM,1800nm}$ [Ω^{-1}]
ITO	Sputtering	5600	0.03	N/A
PEDOT:sulfate	o-CVD (H₂SO₄)	4050	0.003	0.01
PEDOT:PSS*	Spin coat, DMSO	1000	0.0025	0.0004
PEDOT (FeCl ₃) ^[37]	o-CVD (FeCl ₃)	3700	N/A	N/A

metallic conductor, which offers in addition the advantage of a straightforward, facile processing all potentially interesting for industrial large-area applications.

Prior reports of conductive polymers have referred to the potential for metallic transport; however, practical objections such disadvantageous processing and doping-related localization have led to disorder-governed systems finally limiting conductivity. We sought to overcome this limits by a quasi-1-step deposition technique, which we adapted from inorganic semiconductors. Our o-CVD grown PEDOT:sulfate opens various new prospects. Based on enhancement of the local order it assesses the metallic regime offering high conductivity as shown by low temperatures studies on the Hall effect and magneto-electronic interactions. PEDOT-based conducting polymers are commonly used materials in transistors, electrodes, and related optoelectronic devices. In view of the growing interest, our work has substantial impact, as we push the system closer to the MIR limit with keeping its optical transparency. These insights open prospects toward highly conducting polymers based on facile, quasi-1-step processing technique. The new materials offer the possibility of low-cost transparent conductive materials of particular interest to the display- and solar industries.

Experimental Section

For the low-*T* measurements, sapphire with Cr/Au contacts was used. For optical and spectroscopic measurements, glass served as substrate. They were cleaned using ultrasonic bath 15 min each in acetone, isopropyl alcohol, Hellmanex-detergent (Hellma, 70 °C), and deionized water. The metal-contacts were deposited using physical vapor deposition (PVD) through a van-der-Pauw and a four-in-line contact-mask, respectively (Figure 3c, Figure 4b). In order to apply o-CVD for PEDOT:sulfate, following protocol was used. In a tube furnace (Carbolite company, glass tube length: 45 cm, tube thickness inside: 2.4 cm), the substrates were loaded onto a glass holder (Figure 1c), and inserted at the end of the tube (at 40–43 cm). 1 mL of sulfuric acid (97%) is mixed with 1 g of sodium sulfate and loaded into the middle of the tube (20–25 cm). The exhaust gas was flushed through a potassium hydroxide solution to capture residual acid-fumes. Before starting the reaction, the tube was flushed with pure N₂ gas at 200 °C at 0.083 m³ h⁻¹. Then the carrier gas (N₂) was bubbled through a reservoir of EDOT to start the reaction. This time was designated as reaction start. Depending on flow rate and reaction time, films of different thickness were achieved. An example for possible reaction times and corresponding thickness can be found in Table 2 (see the Supporting Information). To stop the reaction, the tube was retrieved from the furnace but kept under N₂-flow in order to cool the samples before exposure to air. After cooling to room temperature, the samples were removed from the tube and washed with isopropyl alcohol.

The samples were stored under inert conditions to avoid humidity. Before electrical characterization, the samples were sealed by drop casting a poly(methyl methacrylate) (PMMA) film on top of the active area. For testing magnetoconductivity, van-der-Pauw geometry and four-probe structured patterned substrates were used with consistently 140–155 nm thin films. For comparison, films of PEDOT:triflate, PEDOT:PSS (and PEDOT:PSS*, respectively) were processed using following recipe: PH1000 (Clevios) dispersion (as-is, PEDOT:PSS and mixed with 5% DMSO, PEDOT:PSS*) were spin-coated to thin films using the following recipe: 10 rps, 2 s ramp, 30 s spinning; 100 rps, 2 s ramp, 30 s spinning. For the PEDOT:triflate, PEDOT:PSS was cast to a thin film and in a second step exposed to excess triflic acid (1:1 molar in water) for 1 min and washed 3 times with 18 M Ω cm water. The resulting solution-based thin films had a comparative thickness of 140 nm (similar to the oCVD-processed thin films). These films were characterized by variable-angle spectroscopic ellipsometry (VASE, Wollam M-2000 with rotating compensator ellipsometer) and modeled using ω VASE program. For fitting Gaussian oscillators have been used, the IR part was fitted by a Tauc-Lorentz dielectric function. All of these model functions were Kramers–Kronig consistent. Atomic force microscopy (AFM) was performed using an Asylum Research MFP-3D Stand Alone AFM. For XPS (Theta Probe from Thermo Fisher Scientific with monochromatic AlK α X-ray source), glass substrates were covered with Cr/Au (Cr 8 nm, Au 100 nm) prior PEDOT-deposition (spin coating at 100 rps, 100 s). XPS surveys as well as high-resolution spectra of the C1s, O1s, S2p peaks were acquired from films with a nominal thickness of 20 nm. The S2p peaks were used to calculate the stoichiometry between PEDOT and PSS or sulfate, respectively. The S2p response from the thiophene ring and the PSS or sulfate was distinctively different ($\Delta = 4$ eV), while the S2p signals from sulfonate and sulfate were practically identical. Solid-state nuclear magnetic resonance (NMR) measurements were taken on a Bruker Avance III 500 MHz spectrometer equipped with a cross-polarization magic-angle spinning (MAS) probe. ¹³C MAS spectra were recorded at 125 MHz at a spinning rate of 17 kHz at a temperature of 298 K. For matrix-assisted laser desorption/ionization–mass spectrometry (MALDI-MS) samples were prepared by intensive mixing with an 100-fold excess of dithranol (1,8,9-Anthracenetriol) in an agate mortar and transferring an aliquot with a spatula onto a ground steel target. The mass spectra were recorded on a Bruker Autoflex III Smartbeam in linear mode with a scan range from 1000 to 4000 *m/z*. For each measurement, 2500–3500 individual spectra were averaged and baseline corrected. All X-ray diffraction (XRD) measurements were performed using Philips Pro X'Pert system working in Bragg-Bretano geometry with CuK α radiation. ATR-FTIR (attenuated total reflection - Fourier transform infrared) spectral measurements were performed using a Bruker IFS66/S spectrophotometer. The exact spectral measurements were conducted on ATR-ZnSe crystals (parallelepiped 1 × 1 cm²) in the near- and mid-IR spectral regime. For the electrical measurements, the van-der-Pauw method was used to detect the Hall potential. For the magnetoconductivity, classic four-in-line probe contacts were used. The PMMA-covered PEDOTs were contacted using indium solder and loaded to the magnetotransport system (DynaCool PPMS, QuantumDesign). The electrical resistivity (thus conductivity) ρ_{xx} and ρ_{xy} were characterized as function of temperature and magnetic field between 300 and 1.8 K and 0 to 9 T, respectively.

Supporting Information

Supporting Information is available from the Wiley Online Library or from the author.

Acknowledgements

P.S., N.S.S., and D.F. are grateful to OEAD (WTZ, IN10/2015) and the Austrian Fund for Advancement of Science (FWF) within the Wittgenstein Prize scheme (Z222-N19 Solare Energieumwandlung) for financial support. The authors thank Eitan Ehrenfreund and Eric D. Głowacki for fruitful discussions. C.C.M., A.W.H., T.G., and D.S. gratefully

acknowledge the financial support by the Austrian Federal Ministry of Science, Research and Economy and the National Foundation for Research, Technology and Development in the frame of the Christian Doppler Laboratories COMBOX and MS-MACH, respectively.

Conflict of Interest

The authors declare no conflict of interest.

Keywords

Anderson localization, conductive metallic polymers, infrared transparency, Mott–Ioffe–Regel limit, transparent conductive electrodes

Received: February 6, 2017

Revised: March 8, 2017

Published online: April 25, 2017

- [1] P. Stadler, D. Farka, H. Coskun, E. D. Głowacki, C. Yumusak, L. M. Uiberlacker, S. Hild, L. N. Leonat, M. C. Scharber, P. Klapetek, R. Menon, N. S. Sariciftci, *J. Mater. Chem. C* **2016**, *4*, 6982.
- [2] C. Cobet, J. Gasiorowski, R. Menon, K. Hingerl, S. Schlager, M. S. White, H. Neugebauer, N. S. Sariciftci, P. Stadler, *Sci. Rep.* **2016**, *6*, 35096.
- [3] N. Massonnet, A. Carella, A. de Geyer, J. Faure-Vincent, J.-P. Simonato, *Chem. Sci.* **2015**, *6*, 412.
- [4] K. Lee, S. Cho, S. H. Park, A. J. Heeger, C.-W. Lee, S.-H. Lee, *Nature* **2006**, *441*, 65.
- [5] M. Ahlskog, R. Menon, A. J. Heeger, T. Noguchi, T. Ohnishi, *Phys. Rev. B* **1997**, *55*, 6777.
- [6] M. N. Gueye, A. Carella, N. Massonnet, E. Yvenou, S. Brenet, J. Faure-Vincent, S. Pouget, F. Rieutord, H. Okuno, A. Benayad, R. Demadrille, J.-P. Simonato, *Chem. Mater.* **2016**, *28*, 3462.
- [7] H. C. F. Martens, J. A. Reedijk, H. B. Brom, D. M. de Leeuw, R. Menon, *Phys. Rev. B* **2001**, *63*, 73203.
- [8] R. Menon, K. Väkiparta, Y. Cao, D. Moses, *Phys. Rev. B* **1994**, *49*, 16162.
- [9] O. Bubnova, Z. U. Khan, H. Wang, S. Braun, D. R. Evans, M. Fabretto, P. Hojati-Talemi, D. Dagnelund, J.-B. Arlin, Y. H. Geerts, S. Desbief, D. W. Breiby, J. W. Andreasen, R. Lazzaroni, W. M. Chen, I. Zozoulenko, M. Fahlman, P. J. Murphy, M. Berggren, X. Crispin, *Nat. Mater.* **2013**, *13*, 190.
- [10] A. Aleshin, R. Kiebooms, R. Menon, A. J. Heeger, *Synth. Met.* **1997**, *90*, 61.
- [11] R. Menon, C. O. Yoon, D. Moses, Y. Cao, A. J. Heeger, *Synth. Met.* **1995**, *69*, 329.
- [12] R. Menon, C. O. Yoon, D. Moses, A. J. Heeger, Y. Cao, *Phys. Rev. B* **1993**, *48*, 17685.
- [13] A. J. Heeger, *J. Phys. Chem. B* **2001**, *105*, 8475.
- [14] A. J. Heeger, N. S. Sariciftci, E. B. Namdas, *Semiconducting and Metallic Polymers*, Oxford University Press, Oxford, UK **2011**, Vol. 21, pp. 391.
- [15] Y. Nogami, H. Kaneko, H. Ito, T. Ishiguro, T. Sasaki, N. Toyota, A. Takahashi, J. Tsukamoto, *Phys. Rev. B* **1991**, *43*, 11829.
- [16] H. H. S. Javadi, A. Chakraborty, C. Li, N. Theophilou, D. B. Swanson, A. G. MacDiarmid, A. J. Epstein, *Phys. Rev. B* **1991**, *43*, 2183.
- [17] D. Jérôme, *Chem. Rev.* **2004**, *104*, 5565.
- [18] B. J. Powell, R. H. McKenzie, *J. Phys.: Condens. Matter* **2006**, *18*, R827.
- [19] R. S. Manna, M. de Souza, A. Brühl, J. A. Schlueter, M. Lang, *Phys. Rev. Lett.* **2010**, *104*, 16403.
- [20] P. Lunkenheimer, J. Müller, S. Krohns, F. Schrettle, A. Loidl, B. Hartmann, R. Rommel, M. de Souza, C. Hotta, J. A. Schlueter, M. Lang, *Nat. Mater.* **2012**, *11*, 755.
- [21] J. E. Frommer, *Acc. Chem. Res.* **1986**, *19*, 2.
- [22] B. J. Worfolk, S. C. Andrews, S. Park, J. Reinspach, N. Liu, M. F. Toney, S. C. B. Mannsfeld, Z. Bao, *Proc. Natl. Acad. Sci. USA* **2015**, *112*, 14138.
- [23] B. Chapman, R. G. Buckley, N. T. Kemp, A. B. Kaiser, D. Beaglehole, H. J. Trodahl, *Phys. Rev. B* **1999**, *60*, 13479.
- [24] T.-R. Chou, S.-H. Chen, Y.-T. Chiang, Y.-T. Lin, C.-Y. Chao, *J. Mater. Chem. C* **2015**, *3*, 3760.
- [25] Y. Xia, K. Sun, J. Ouyang, *Adv. Mater.* **2012**, *24*, 2436.
- [26] C. M. Palumbiny, F. Liu, T. P. Russell, A. Hexemer, C. Wang, P. Müller-Buschbaum, *Adv. Mater.* **2015**, *27*, 3391.
- [27] Q. Wei, M. Mukaida, Y. Naitoh, T. Ishida, *Adv. Mater.* **2013**, *25*, 2831.
- [28] J. Y. Kim, J. H. Jung, D. E. Lee, J. Joo, *Synth. Met.* **2002**, *126*, 311.
- [29] J.-Y. Kim, M.-H. Kwon, Y.-K. Min, S. Kwon, D.-W. Ihm, *Adv. Mater.* **2007**, *19*, 3501.
- [30] J. Huang, P. F. Miller, J. C. de Mello, A. J. de Mello, D. D. C. Bradley, *Synth. Met.* **2003**, *139*, 569.
- [31] C. S. S. Sangeeth, M. Jaiswal, R. Menon, *J. Appl. Phys.* **2009**, *105*, 63713.
- [32] S. K. Jönsson, J. Birgersson, X. Crispin, G. Greczynski, W. Osikowicz, A. D. van der Gon, W. Salaneck, M. Fahlman, *Synth. Met.* **2003**, *139*, 1.
- [33] X. Crispin, F. L. E. Jakobsson, A. Crispin, P. C. M. Grim, P. Andersson, A. Volodin, C. Van Haesendonck, M. Van Der Auweraer, W. R. Salaneck, M. Berggren, *Chem. Mater.* **2006**, *18*, 4354.
- [34] B. Winther-Jensen, J. Chen, K. West, G. Wallace, *Macromolecules* **2004**, *37*, 5930.
- [35] A. M. Coclite, R. M. Howden, D. C. Borrelli, C. D. Petruczkow, R. Yang, J. L. Yagüe, A. Ugur, N. Chen, S. Lee, W. J. Jo, A. Liu, X. Wang, K. K. Gleason, *Adv. Mater.* **2013**, *25*, 5392.
- [36] P. Kovacic, G. del Hierro, W. Livernois, K. K. Gleason, *Mater. Horiz.* **2015**, *2*, 221.
- [37] A. Ugur, F. Katmis, M. Li, L. Wu, Y. Zhu, K. K. Varanasi, K. K. Gleason, *Adv. Mater.* **2015**, *27*, 4604.
- [38] H. Meng, D. F. Perepichka, F. Wudl, *Angew. Chem.* **2003**, *115*, 682.
- [39] S. Lee, K. K. Gleason, *Adv. Funct. Mater.* **2015**, *25*, 85.
- [40] K. Kang, S. Watanabe, K. Broch, A. Sepe, A. Brown, I. Nasrallah, M. Nikolka, Z. Fei, M. Heeney, D. Matsumoto, K. Marumoto, H. Tanaka, S. Kuroda, H. Sirringhaus, *Nat. Mater.* **2016**, *15*, 896.
- [41] J. H. Mooij, *Phys. Status Solidi* **1973**, *17*, 521.
- [42] P. A. Lee, T. V. Ramakrishnan, *Rev. Mod. Phys.* **1985**, *57*, 287.
- [43] C. C. Tsuei, *Phys. Rev. Lett.* **1986**, *57*, 1943.
- [44] T. J. Wood, P. S. Brown, J. P. S. Badyal, *Chem. Commun.* **2013**, *49*, 7741.
- [45] E. B. Aleksandrov, I. V. Sokolov, A. Gatti, M. I. Kolobov, L. A. Lugiatto, T. A. Vartanyan, *Usp. Fiz. Nauk* **2001**, *171*, 1263.
- [46] P. W. Anderson, *Phys. Rev.* **1958**, *109*, 1492.
- [47] N. F. Mott, *Philos. Mag.* **1972**, *26*, 1015.
- [48] A. B. Kaiser, *Rep. Prog. Phys.* **2001**, *64*, 1.
- [49] R. Menon, *Synth. Met.* **1996**, *80*, 223.
- [50] G. Bergmann, *Phys. Rep.* **1984**, *107*, 1.
- [51] G. Bergmann, *Phys. Rev. B* **1983**, *28*, 2914.
- [52] T. F. Rosenbaum, R. F. Milligan, G. A. Thomas, P. A. Lee, T. V. Ramakrishnan, R. N. Bhatt, K. DeConde, H. Hess, T. Perry, *Phys. Rev. Lett.* **1981**, *47*, 1758.
- [53] A. Kawabata, *Solid State Commun.* **1980**, *34*, 431.
- [54] R. Kubo, *J. Phys. Soc. Jpn.* **1957**, *12*, 570.
- [55] L. Friedman, N. F. Mott, *J. Non-Cryst. Solids* **1972**, *7*, 103.
- [56] L. Friedman, *J. Non-Cryst. Solids* **1971**, *6*, 329.
- [57] G. Haacke, *J. Appl. Phys.* **1976**, *47*, 4086.